Energetics of Xylose Decomposition as Determined Using Quantum Mechanics Modeling

Mark R. Nimlos,*,† Xianghong Qian,‡ Mark Davis,† Michael E. Himmel,† and David K. Johnson†

National Bioenergy Center, National Renewable Energy Laboratory, Golden, Colorado 80401, and Rx-Innovation, Inc., Fort Collins, Colorado 80525

Received: May 2, 2006; In Final Form: August 7, 2006

The decomposition of xylose has been studied using quantum mechanical calculations supported by NMR data. Proposed mechanisms for the decomposition of xylose have been investigated by obtaining the structures and energies of transition states and products. The intent of this study was to understand the experimentally observed formation of furfural and formic acid that occurs during the decomposition of xylose in mildly hot acidic solutions. A mechanism of furfural formation involving the opening of the pyranose ring and subsequent dehydration of the aldose was compared to a direct intramolecular rearrangement of the protonated pyranose. Energies were determined using CBS-QB3, and it was shown that the barriers for dehydration of the aldose were high compared to intramolecular rearrangement. This result suggests that the latter mechanism is a more likely mechanism for furfural formation. The intramolecular rearrangement step results from protonation of xylose at the O2 hydroxyl group. In addition, it has been shown that formic acid formation is a likely result of the protonation of xylose at the O3 hydroxyl group. Finally, solvation of xylose decomposition was studied by calculating energy barriers for xylose in selected water clusters. The mechanisms proposed here were supported in part by ^{13}C-labeling studies using NMR.

Introduction

Sugars are critical for many biological processes and essential building blocks for the biopolymers that make up plant cell walls. As such, their chemistry is central for understanding plant cell wall function and structure. In addition, sugars isolated from plant matter represent an important renewable feedstock for the production of chemicals and fuels.[1,2] A deep understanding of the chemical reaction mechanisms and kinetics of sugar degradation is thus key to development of a sustainable renewable industry.[3] The most prevalent sugar found in plant mater is glucose, which is the monomer of cellulose. Cellulose chains form the core of the microfibrils that give plant cell walls their structure and strength. Xylose, **1**, is also an important sugar in the structure of these microfibrils and the plant cell wall matrix. This pentosan has an orientation of hydroxyl groups similar to glucose in its pyranose form, but is missing the terminal $-CH_2OH$ group. Xylose is the building block monosaccharide of xylan and other hemicelluloses that coat the crystalline cellulose cores of cell wall microfibrils, which constitute roughly 30% of plant matter.[4]

As a result of its importance, numerous studies of the structure and reactivity of glucose are available. Experimental measurements of the structure and conformational energetics also exist. This is also an active area of research for molecular modeling[5−17] using either quantum mechanics or molecular mechanics. There is less information available, however, concerning the reaction mechanisms for glucose degradation and conversion. Although it is also an important sugar in nature, there exists even less information concerning the structure and reactivity of xylose.

In particular, the mechanisms of degradation of glucose and xylose during the acid hydrolysis of plant matter remain unclear. Dilute acid hydrolysis (i.e., 1−2 wt % H_2SO_4) at moderate temperatures (<200 °C) is a commonly used procedure for hydrolyzing the ether linkages between hemicellulosic sugar molecules as a conditioning step to make plant biomass more amenable to enzyme conversion to fermentable sugars.[18] These mildly acidic conditions are also known to lead to the decomposition of xylose and, to a much lesser extent, glucose.[19,20] The main products from acid degradation of these sugars are furfuraldehydes as is shown in the reaction below. In fact, acid hydrolysis is used as an industrial process to produce furfural from xylan in oat hulls.[21]

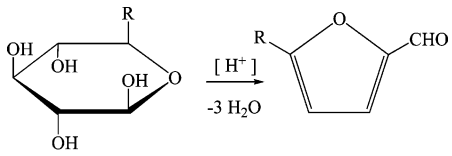

R = H, Xylose
R = CH_2OH, Glucose

The decomposition of xylose in acidic solutions has been the focus of a number of studies dating back[22] to the 1930s. Furfural, **7**, is the main product from this decomposition. Initially, the mechanism for furfural formation was proposed[23−25] to occur from the open form of the sugar, **2**, as is shown in Scheme 1. In this scheme, the cyclic structure of xylose opens to the aldose form, **2**, which then isomerizes and dehydrates to give **6**. This compound can then dehydrate to furfural.

More recently, two mechanisms were proposed[26] which involved direct rearrangement of the cyclic structure after protonation and dehydration. These are shown in Schemes 2 and 3.

In Scheme 2, the oxygen attached to carbon number 1, O1, is protonated, **8**, and loses a water molecule to form an oxonium

† National Renewable Energy Laboratory.
‡ Rx-Innovation, Inc.

10.1021/jp0626770 CCC: $33.50
Published on Web 10/04/2006

SCHEME 1

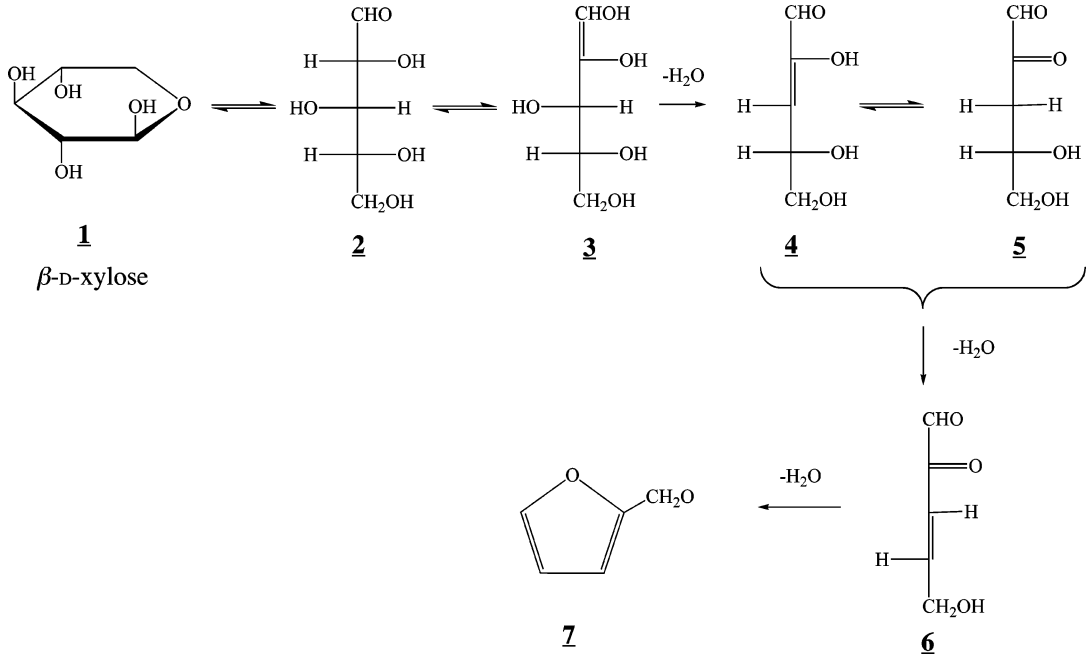

SCHEME 2

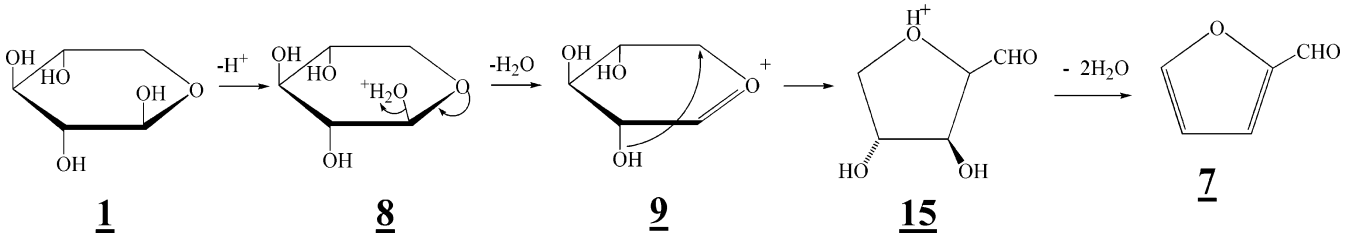

SCHEME 3

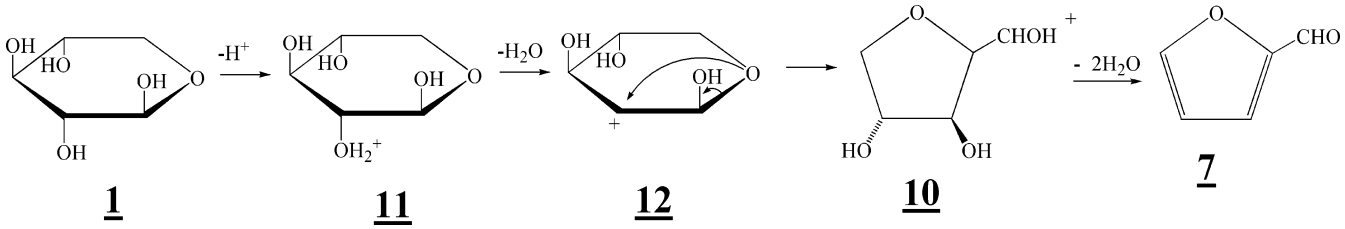

ion, **9**. The O2 hydroxyl adds to C5 to form the dehydrofuranose, **15**, which then dehydrates twice to form furfural, **7**. In Scheme 3, **7** is formed by protonation of **1** at O2 (**11**), followed by loss of water from C2 (**12**), attack of O5 on the resulting carbocation (**10**), and loss of two additional water molecules. These mechanisms resemble earlier mechanistic work[27] by Shafizadeh *et al.* Formic acid has also been measured[21] as a product of xylose decomposition in hot dilute acid, but no mechanisms have been proposed for its formation. Under more severe conditions, 250 °C, other products[26] were measured. The reactions leading to the formation of these products may be due to mechanisms that are more complicated than unimolecular decomposition. Kinetic studies of the conversion of xylose into furfural have also been reported, and activation energies of 32 and 30.3 kcal mol^{-1} have been reported.[28,29]

Despite the importance of xylose decomposition and its long industrial use, the mechanism of its decomposition is still not fully understood. Previously, quantum mechanical molecular dynamics simulations[30] have been conducted on protonated xylose in order to simulate the reaction of this species in an acidic environment. Calculations were conducted in which a proton was attached in turn to each of the five oxygen atoms in a vacuum, and it was found that the reactivity and the products were dependent on the site of protonation. Protonating the number two oxygen, O2, resulted in the formation of the dehydrofuranose, **10**, as shown in Scheme 3, whereas protonation on O3 resulted in the formation of a precursor to formic acid. Protonation of the other oxygen atoms resulted in no reaction during the 2 ps simulations. Though this study seemed to show that Scheme 3 was operative for furfural formation, transition states or energy barriers were not obtained. In addition, because these simulations are computationally demanding, only the first steps in these reactions could be investigated using *ab initio* molecular dynamics Car−Parrinello molecular dynamics (CPMD). The Car−Parinello method combines molecular dynamics and density functional theory and is used to optimize geometries, find saddle points, and perform relatively short *ab initio* molecular dynamics simulations.[31] To evaluate the mechanisms in Schemes 1−3, calculations should be performed on all of the reaction steps.

In this study, the reaction mechanisms for the acid-catalyzed decomposition of xylose were investigated further using quantum molecular modeling. The proposed mechanisms shown in Schemes 1−3 were evaluated by calculating reaction energy barriers for the entire mechanism. In addition, the energy barriers for the reactions that lead to the formation of formic acid were calculated. The approach used here was to study the decomposition of xylose protonated at each of its hydroxyl groups. As part of this investigation, we report NMR measurements of products from the decomposition of isotopically labeled xylose. Finally, the effect of explicit water molecules upon reaction barriers was investigated and compared to experimental results.

Computational Approach

Quantum calculations were used to obtain energies for reactants and transition states and products so that reaction energies and barriers could be obtained. We used the *Gaussian03*[32] suite of programs, running on a Linux cluster, that were designed to obtain minima in potential energy surfaces corresponding to stable molecular species and saddle points that correspond to transition states. Hybridized density functional theory, B3LYP, and complete basis set,[33] CBS, extrapolation were used. Energies were obtained with CBS-QB3, which optimizes the geometry at the B3LYP/6-311G(d,p) level and extrapolates the energy to the complete basis set limit for MP2. Others have compared results from these techniques to experimental measurements for the G2 set[34] and found that the standard deviations are about ±3 kcal mol^{-1} for the B3LYP technique[35] and ±1.5 kcal mol^{-1} for the CBS technique.[33] The B3LYP technique can underestimate transition states[36−40] by up to ±5 kcal mol^{-1}, while the CBS technique provides more accurate results.[36,41] The starting geometries for stable species were selected from the low-energy conformers from previous CPMD calculations and literature results. The optimized geometries had no imaginary vibrational frequencies. Results from earlier CPMD calculations also helped guide the selection of reaction pathways to be studied. Transition states in these mechanisms had exactly one imaginary frequency and were confirmed by visual inspection and by intrinsic reaction coordinate (IRC) calculations.[42,43] Reaction energy barriers, E_a, were determined as the difference in potential energy of the transition state and the reactant including zero point energy, $\Delta_{TS}E_{0K}$.

Xylose Struture. Calculations of D-xylose in this study were limited to the chair conformation designated[44] as $^4C_1$, in which all of the hydroxyl groups are in the equatorial position. This structure has been experimentally observed in the crystal structures of α- and β-D-xylose.[45,46] Quantum mechanical calculations[44] predict that this structure is more stable than the chair $^1C_4$ structure (where the hydroxyl groups are axial) by about 8 kcal mol^{-1} in glucose. In this study, we used a xylose structure in which the OH groups all point in the same direction around the pyranose ring toward O5. According to the convention adopted by Cramer and Thrular,[29] this conformation is named *gḡḡg* and for glucose and is also calculated to be the lowest-energy conformer[17,47] for that molecule. The *gḡḡg* structures for β- and α-D-xylose are shown in Figure 1 as determined using B3LYP/6-311G(d,p). The calculated hydrogen bond lengths are also shown. CBS-QB3 calculations predict that the energy of this conformation is 2.6 kcal mol^{-1} lower than the clockwise orientation for β-D-xylose and 1.8 kcal mol^{-1} lower for α-D-xylose. Similar differences were obtained for glucose.[17,47,48]

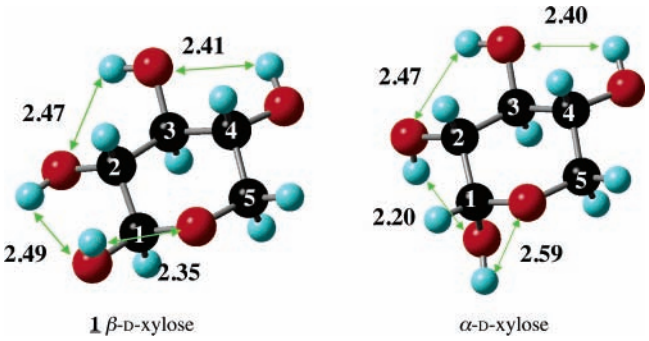

Figure 1. Structures of β-D-xylose (top left) and α-D-xylose (top right) from B3LYP/6-311G(d,p). Calculated internal hydrogen bond lengths are shown.

TABLE 1: Calculated Bond Lengths[a] for Xylose

	β-D-xylose		α-D-xylose	
	DFT[b]	crystal[c]	DFT[b]	crystal[d]
C1−C2	1.53	1.519(13)	1.54	1.531
C2−C3	1.52	1.537(13)	1.52	1.529
C3−C4	1.52	1.527(13)	1.52	1.515
C4−C5	1.53	1.525(13)	1.53	1.503
C5−O5	1.43	1.455(11)	1.43	1.449
O5−C1	1.42	1.424(11)	1.40	1.428
C1−O1	1.40	1.405(11)	1.41	1.393
C2−O2	1.42	1.419(11)	1.42	1.475
C3−O3	1.42	1.424(11)	1.42	1.418
C4−O4	1.42	1.431(11)	1.43	1.411

[a] Bond lengths in angstroms. [b] B3LYP/6-311G(d,p). [c] ref 46. [d] ref 45.

Table 1 compares the calculated values of bond lengths for the heavy atoms of these species to the experimental values measured using X-ray crystallography.[45,46] As can be seen, the agreement between calculated and experimental values is within 0.03 Å. Similar agreement was found for the bond angles. CBS calculations predict that, in a vacuum, the α-pyranose form of the sugar is 1.5 kcal mol^{-1} lower in energy than the β-pyranose form. This is contrary to experimental measurements in solution,[49] which have shown that the β-pyranose is favored. However, the CBS calculations are consistent with other gas-phase calculations of glucose[47] and with CPMD calculations.[30]

Results and Discussion

Addition of Protons to Oxygen Atoms. The degradation of xylose in acid was modeled by following the unimolecular reaction mechanisms after a proton was added to each of its hydroxyl groups. The relative barrier energies of the competing reaction channels were then compared. Figure 2 shows an overall scheme of the reactions that are presented here. Calculated activation energies are shown in this picture. Other pathways were found to have barriers too high to be considered important and are not discussed. Though it is likely that all possible reactions have not been considered, the results of the calculations for these pathways are consistent with experimental evidence and CPMD calculations. The results show that protonation at O1 readily leads to a stable oxonium ion and that the barrier for the reaction in Scheme 1, $E_a = 32$ kcal mol^{-1}, is too high to make this reaction likely. Protonation at O2 can lead through a series of dehydration and unimolecular rearrangement reactions to protonated furfural, which is consistent with Scheme 2. Protonation at O3 can lead to the formation of formic acid, which has been observed elsewhere and in this work. Protonation at O4 leads to water loss and a product that is readily converted back to xylose. Finally, protonation at O5

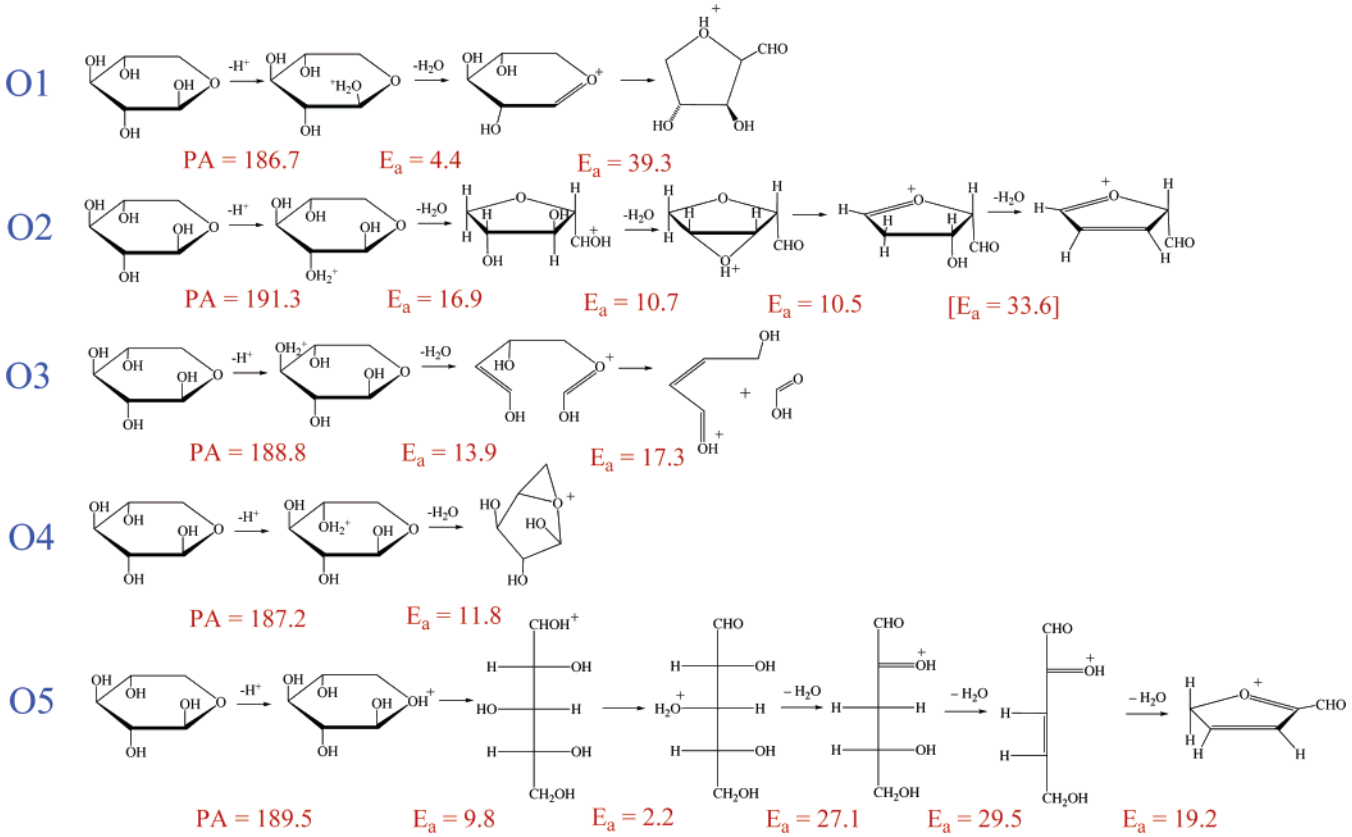

Figure 2. Reaction scheme showing the reaction of xylose protonated at different oxygen atoms (shown in blue). The proton affinities, PA, and the activation energies, E_a, are in kcal mol^{-1} and were determined using CBS-QB3. Note that the activation energy in square brackets for O2 can be overcome by chemical activation energy (see Figure 5).

TABLE 2: Calculated[a] Proton Affinities (PA) of Xylose

protonation site	PA (kcal mol^{-1})
O1	186.7
O2	191.3
O3	188.8
O4	187.2
O5	189.5

[a] CBS-QB3.

can lead to ring opening, rearrangement, dehydration, and furfural formation. However, the barriers for these reactions are too high to be competitive with furfural formation from protonation at O2. As mentioned, details concerning the calculations for each step in these sequences will be presented below.

Proton Affinities. The energy of proton addition is an important first step in these mechanisms. Proton addition in the gas phase is typically a barrierless process and can be characterized by the proton affinity, PA, or the standard enthalpy of abstraction of H^+ from the protonated molecule. Table 2 presents the PAs calculated using CBS-QB3, and the PAs are also shown in Figure 2. By comparison, the proton affinity of H_2O is calculated to be PA = 162.5 kcal mol^{-1}, which compares well with the experimental value[9] of 165 kcal mol^{-1}. As can be seen from the table, O2 has the largest proton affinity, 191.3 kcal mol^{-1}, and this oxygen atom is the most likely site for proton addition. Protonation at the O1 is the least likely, since the PA at this site is 186.7 kcal mol^{-1}. This range of PAs is consistent with the experimental and calculated PAs of secondary alcohols. For instance, the experimental[50] PA of 2-propanol is 189.5 kcal mol^{-1}, and the value calculated[41] using CBS-QB3 is 187.1 kcal mol^{-1}.

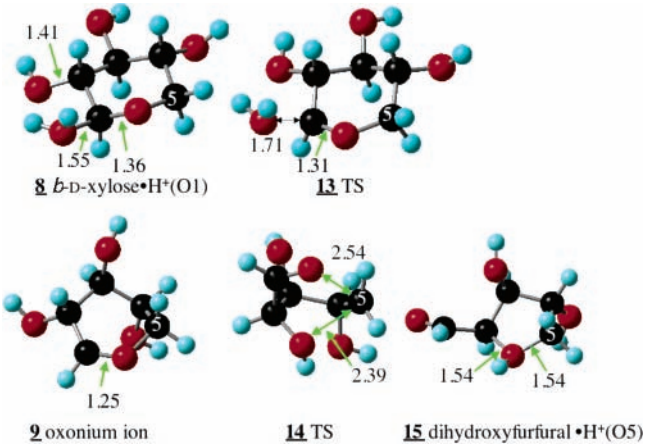

Figure 3. Structures of the species involved in the reaction of xylose protonated at O1. Structures were determined using B3LYP/6-311G-(d,p), and selected bond lengths are shown.

Reactions of Xylose Protonated at O1. As shown in reaction 1, protonation of xylose at O1, **8**, allows a simple dehydration to form the stable oxonium ion, **9**. In this reaction, the transition state is shown schematically as **13**. Loss of water from a cation will necessarily involve the formation of a water/cation cluster, which has a lower energy than the energy of the product and a separated water molecule. Reaction 1 also shows a schematic picture of the water cluster. *Note that, in dehydration reactions in the remainder of this manuscript, the cluster will not be shown.* The energies of the water clusters were also calculated in this study, and the structures and energies are collected in the Supporting Information. No attempt is made to obtain the

global energy minimum of the clusters. The energies of the clusters are only included for qualitative comparison. The calculated energy for reaction 1 forming the separated products is $\Delta_{react}E_{0K}$(react 1) = 3.4 kcal mol^{-1}. The energy for the formation of the cluster from the product is $\Delta_{clust}E_{0K}$ (react 1) = −6.7 kcal mol^{-1}. The energy of the transition state, **13**, relative to the reactant is $\Delta_{TS}E_{0K}$ (react 1) = 4.4 kcal mol^{-1}. The structures for these species, with the exception of the cluster, are shown in Figure 3, which also shows selected bond lengths. Addition of a proton to O1 leads to a weaker C1−O1 bond, as is seen by the longer bond in **8**, r_{C1-O1}(**8**) = 1.55 Å, compared to neat xylose, r_{C1-O1}(**1**) = 1.40 Å. As a result of the weakened bond, loss of water to form the oxonium ion is facile. This conclusion is also demonstrated by CPMD calculations,[30] in which the loss of water occurs within 2 ps.

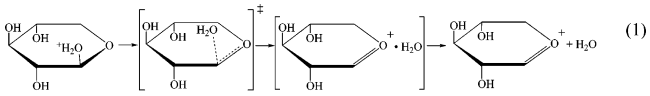

(1)

8 **13** water cluster **9**

In Scheme 2, the oxonium ion, **9**, reacts to form the dehydrofuranose, which could then dehydrate to form furfural. A schematic picture of this reaction with the transition state, **14**, is shown in reaction 2. The structures for **14** and **15** as determined with B3LYP/6-311G(d,p) are shown in Figure 3. The structure of **14** along with the IRC calculation and the imaginary frequency show that **14** connects **9** to **15.** CPMD calculations[30] showed no such reaction of the oxonium ion in 2 ps. Consistent with this, CBS-QB3 calculations predict a high barrier for this reaction. The energy of this reaction was calculated to be $\Delta_{react}E_{0K}$(react 2) = 18.4 kcal mol^{-1}, and the transition-state energy was calculated to be $\Delta_{TS}E_{0K}$(react 2) = 39.3 kcal mol^{-1}. This energy barrier is too high for this reaction to be significant at moderate temperatures (<200 °C), and Scheme 2 is unlikely. The stability of the oxonium ion, **9**, makes other unimolecular decomposition reactions unlikely, as confirmed by CPMD[30] calculations. The energy barriers for reactions 1 and 2 are shown in the schematic in Figure 2. Though reaction 1 to form the oxonium ion should be facile, further reaction is unlikely, and recombination with water should quickly reform xylose resulting in mutarotation.

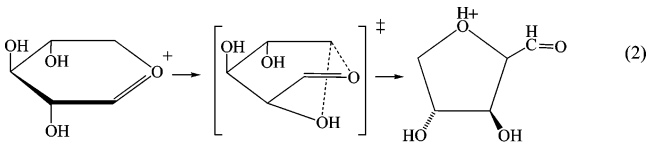

(2)

9 **14** **15**

Reaction of Xylose Protonated at O2. Calculations conducted in this study confirmed that xylose protonated at O2 can decompose as shown in Scheme 3 to form the dehydrofuranose, **10**. These calculations also showed that this product can further be decomposed to form furfural through a series of unimolecular decomposition reactions. This mechanism is shown in Figure 2. The barriers for each of these steps were found to be low compared to other reactions studied, so that this mechanism appears to be a likely explanation for the formation of furfural in acid solutions. Details of each step in this reaction mechanism are provided below.

The first step in this mechanism is a single, concerted reaction involving loss of water and rearrangement as is shown in reaction 3. The calculated energy of this reaction as written is $\Delta_{react}E_{0K}$(react 3) = 20.9 kcal mol^{-1}, whereas formation of the water cluster, which is not shown in reaction 3, has an energy of $\Delta_{clust}E_{0K}$(react 3) = 2.5 kcal mol^{-1}. Figure 4 shows the structure of the reactant, **11**, transition state, **16**, and product, **10**, along with selected bond lengths. As with protonation at O1, **11** has a long C2−O2 bond, r_{C2-O2}(**11**) = 1.54 Å, indicating a weakening of this bond. IRC calculations, the geometry shown in Figure 4, and the imaginary frequency of **16** confirmed that the transition state links **11** to **10**. The calculated energy of the transition state is $\Delta_{TS}E_{0K}$(react 3) = 16.4 kcal mol^{-1}, which indicates that this reaction should be significant at temperatures between 150 and 200 °C.

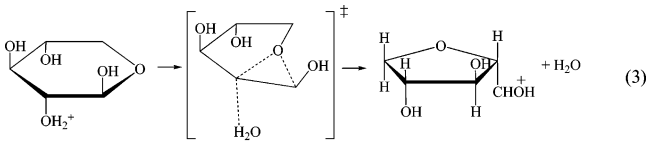

(3)

11 **16** **10**

In order for **10** to be converted to the experimentally observed product (furfural), it must lose two water molecules. Simple 1,2-dehydrations, such as that shown in reaction 4, typically have high reaction barriers. For instance, these types of dehydration reactions applied to simple alcohols have barriers[41,51,52] above 70 kcal mol^{-1}. Attempts to locate these types of barriers were unsuccessful, perhaps because reactions with lower energy barriers are available.

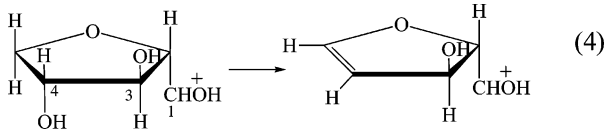

(4)

It is more likely that dehydration would occur after the hydroxyl groups in **10** are protonated. With simple alcohols, protonation of the hydroxyl groups significantly lowered the barriers[41] to 1,2-dehydration. The hydroxyl groups could receive a proton by direct transfer from O1 or by solvent-mediated proton transfer. The ion formed by transferring a proton to O3 is unstable, and the proton spontaneously transfers back to O1, whereas transfer of a proton to O4 produces a stable molecule, **17**. This product has a higher energy than **10** by 4.2 kcal mol^{-1}, though a transition state for this proton transfer could not be located.

Two low-energy dehydration mechanisms were identified for the dihydroxyfurfural protonated at O3 or O4 (reactions 5−8): (1) concerted loss of water and hydride transfer and (2) a substitution reaction in which the neighboring hydroxyl group attacks the carbon atom as the water molecule is leaving. The hydride transfer reactions are shown in reactions 5 and 7 for protonation at O4 and O3. Note that, as mentioned above, when **10** is protonated at O3 an unstable species is formed. This species is shown in parentheses in reactions 7 and 8 for discussion purposes only. The hydride transfer reactions result in the formation of a protonated ketone, **19** and **23**, as shown. Further dehydration would necessarily involve loss of this doubly bound oxygen atom, which would be difficult. In addition, the energies of the transition states for these reactions, **18** and **22**, were found to be approximately 3.5 and 5 kcal mol^{-1} higher than the transition states for the substitution reactions. Thus, the hydride transfer reactions are unlikely, and details of these reactions are not provided here. Structures and energies of the transition states and products can be found in the

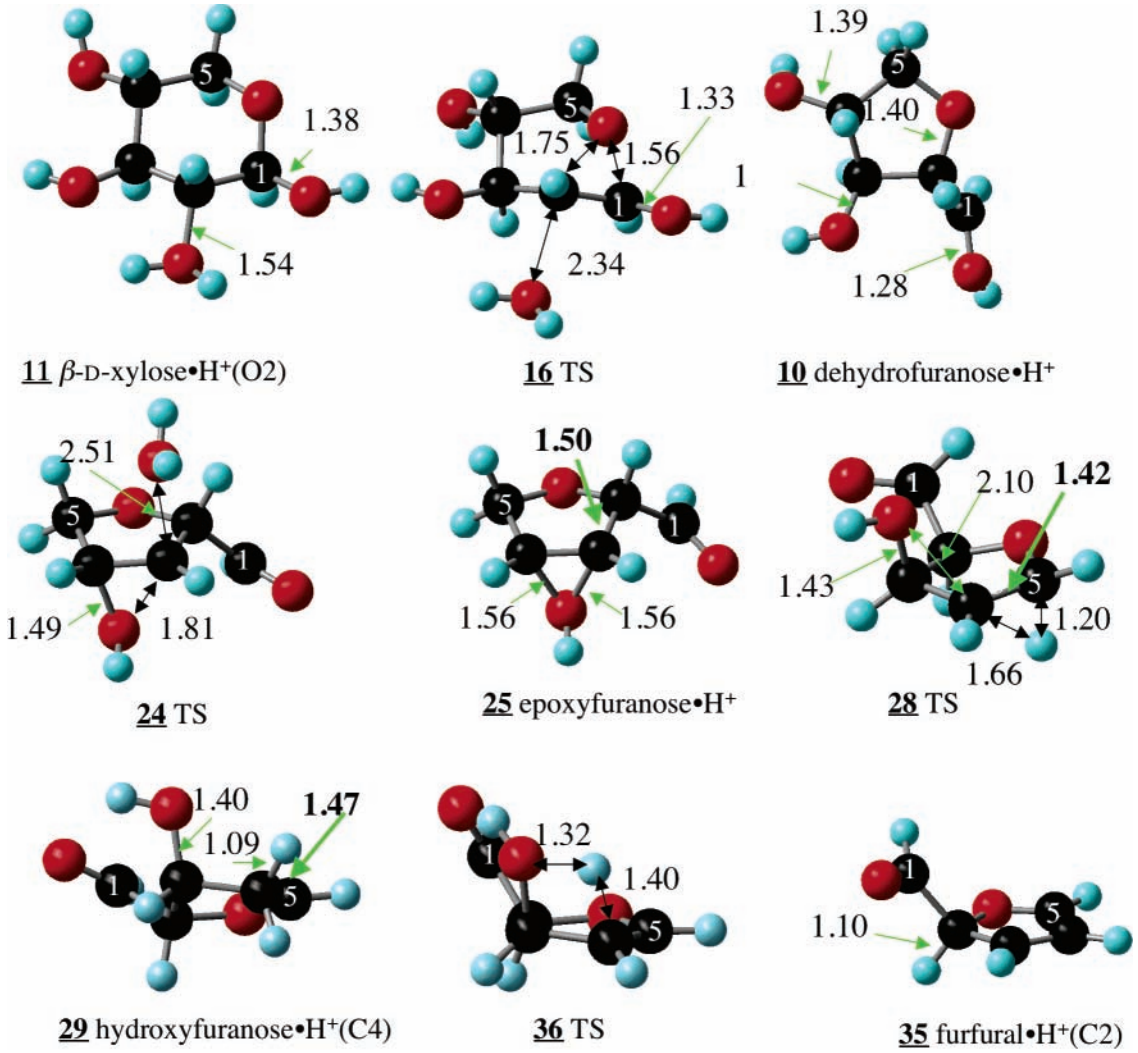

Figure 4. Selected structures for the decomposition of xylose protonated at O2 determined using B3LYP/6-311G(d,p). The species from reactions 3, 8, 10, and 14 are shown. The C4−C5 bond distance is highlighted in bold for the hydride transfer reaction 10 to show that this length is shortened in the transition state. This is due to π-character of this bond in the transition state.[53]

Supporting Information. The substitution reactions, 6 and 8, are similar to those found for glycerol dehydration[53] and result in the formation of an epoxide. The transition state of reaction 6, protonation at O4, had an energy of $\Delta_{TS}E_{0K}$(react 6) = 12.3 kcal mol^{-1} relative to **10**, whereas the transition state for reaction 8 had a relative energy of $\Delta_{TS}E_{0K}$(react 8) = 10.7 kcal mol^{-1}. Thus, both of these reaction pathways are possible at moderate temperatures. The energy for formation of water clusters, relative to **10**, from reactions 6 and 8 are $\Delta_{clust}E_{0K}$(react 6) = 12.1 kcal mol^{-1} and $\Delta_{clust}E_{0K}$(react 8) = 9.5 kcal mol^{-1}, and the reaction energies for these reactions are $\Delta_{react}E_{0K}$(react 6) = 21.1 kcal mol^{-1} and $\Delta_{react}E_{0K}$(react 8) = 20.7 kcal mol^{-1}. The geometries of **24** and **25** from reaction 8 are shown in Figure 4. The atomic coordinates of **17**, **20**, and **21** from reaction 6 are contained in the Supporting Information.

The epoxides formed from reactions 6 and 8 will need to undergo another dehydration to form furfural. This first requires the breaking of the epoxide ring by hydride transfer from adjacent carbon atoms, C2 or C5. The hydrogen anions can transfer syn- or anti-periplanar to the OH leaving group. Reactions 9−11 show the possible anti-periplanar hydride transfer reactions for **21** and **25**. Note that in the anti-periplanar transition states, **26**, **28**, and **30**, the hydride is moving on the opposite side of the plane of the ring as the OH group. For the syn-periplanar transition states, the hydride ion would be on the same side. The anti-periplanar reactions have barriers about 5 kcal mol^{-1} lower than the syn-periplanar reactions, which are not discussed here. For the epoxide **21**, there is only one possible

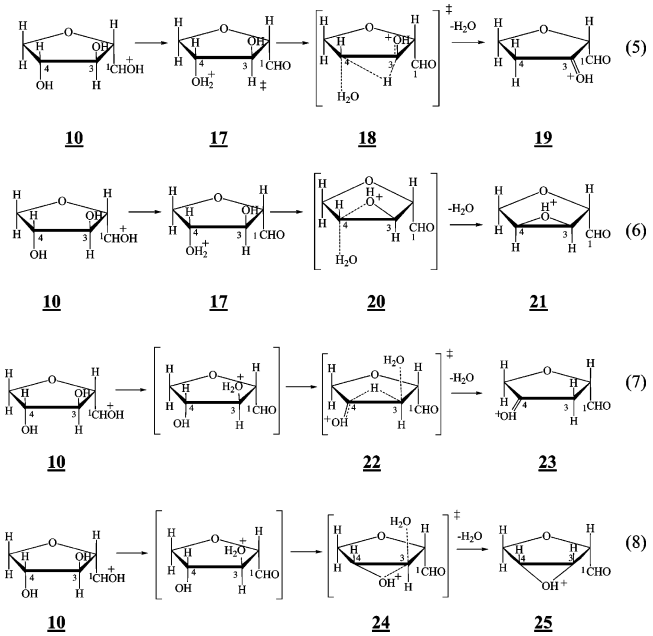

hydride transfer, reaction 9, whereas for **25**, there are two possibilities, reactions 10 and 11. An interesting characteristic of these hydride transfer reactions is that the C−C bond involved in the hydride transfer is shorter in the transition state than in the reactant or the product. This is due to the π-character that must develop in this bond in order for the hydride transfer to occur.[53] For instance, in reaction 10, the C4−C5 bond length in the reactant is r_{C4-C5}(**25**) = 1.50 Å, in the transition state, it is r_{C4-C5}(**28**) = 1.42 Å, and in the product, it is r_{C4-C5}(**29**) = 1.47 Å. Reactions 9−11 are exothermic with energies of $\Delta_{react}E_{0K}$(react 9) = −28.3 kcal mol^{-1}, $\Delta_{react}E_{0K}$(react 10) = −29.3 kcal mol^{-1}, and $\Delta_{react}E_{0K}$(react 11) = −29.9 kcal mol^{-1}; and they have low barriers, $\Delta_{TS}E_{0K}$(react 9) = 8.6 kcal mol^{-1}, $\Delta_{TS}E_{0K}$(react 10) = 10.5 kcal mol^{-1}, and $\Delta_{TS}E_{0K}$(react 11) = 9.5 kcal mol^{-1}. Since these barriers have similar values, each of these reactions is equally likely. The transition state **28** and the product of reaction 10, **29**, are shown in Figure 4. The atomic coordinates for the transition states and products are collected in the Supporting Information.

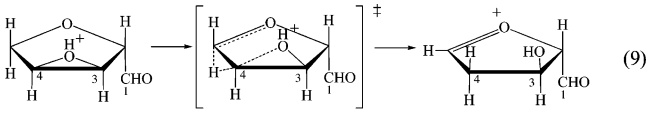

(9)

21 **26** **27**

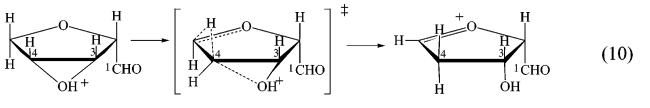

(10)

25 **28** **29**

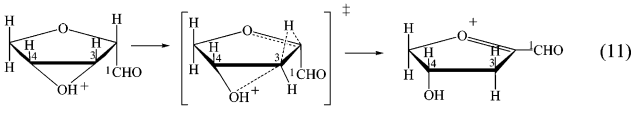

(11)

25 **30** **31**

Further decomposition of **27**, **29**, or **31** to form furfural requires a 1,2-dehydration, which typically has a high activation energy as mentioned above. However, since the product, furfural, is very stable, the calculated barriers are lower than the barriers for typical 1,2-dehydration reactions. Reactions 12−16 show the possible 1,2-dehydration pathways for **27**, **29**, and **31**. Reactions 12 and 16 are unlikely, since they have high energy barriers, $\Delta_{TS}E_{0K}$(react 12) = 50.8 kcal mol^{-1} and $\Delta_{TS}E_{0K}$(react 16) = 57.9 kcal mol^{-1}. Reactions 13−15 have similar barriers of $\Delta_{TS}E_{0K}$(react 13) = 34.3 kcal mol^{-1}, $\Delta_{TS}E_{0K}$(react 14) = 33.6 kcal mol^{-1}, and $\Delta_{TS}E_{0K}$(react 15) = 33.3 kcal mol^{-1}. While these barriers are also high, they are less than the sum of the energy of the barriers and exothermicity of reactions 9−11. Because of this chemical activation energy, reactions 13−15 should be facile. The transition state, **36**, and product, **35**, of reaction 14 are shown in Figure 4. Atomic coordinates for the species in reactions 12, 13, 15, and 16 are collected in the Supporting Information.

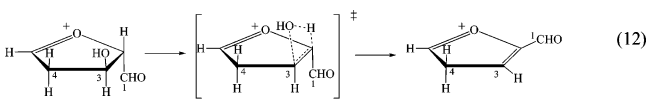

(12)

27 **32** **33**

The results of these calculations show that the formation of furfural from xylose protonated at O2 is feasible. The mechanism consists of a concerted dehydration and rearrangement,

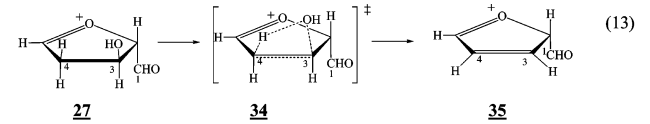

(13)

27 **34** **35**

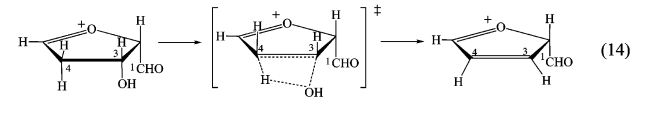

(14)

29 **36** **35**

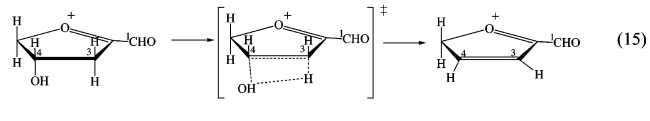

(15)

31 **37** **38**

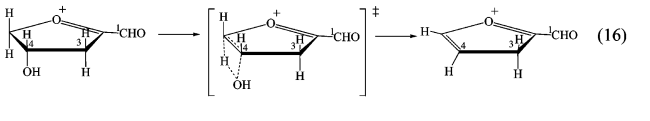

(16)

31 **39** **40**

reaction 3, to form the dihydoxy furanyl compound, followed by dehydration/substitution, reactions 6 and 8, to form an epoxide, a hydride transfer, reactions 9−11, and 1,2-dehydration, reactions 13−15. Each of these reaction steps has barriers lower than 16.4 kcal mol^{-1}, the energy barrier for the first reaction. Thus, this reaction should be the rate-limiting step, which could explain why none of these intermediates have been measured. Figure 5 plots the potential energy of the unimolecular decomposition of xylose·H$^+$(O2) to form furfural. For simplicity, this plot only includes reactions 3, 8, 10, and 14, though the energies for other likely pathways discussed above are similar. Note that the transition from the water cluster of **10**, shown as "[**10**·H_2O]", to **10** + H_2O is indicated with a dotted line. In water solutions, this energy will not be required, since the molecule will be "clustered" by solvent water molecules. Likewise, the transition from clustered **25** to unclustered **25** is shown with a dotted line. As a result, the high overall barrier for xylose conversion to furfural in the gas phase, 52.2 kcal mol^{-1}, should be significantly lower in water. For instance, if we subtract the water cluster energies for **10**, 18.4 kcal mol^{-1}, and **25**, 11.3 kcal mol^{-1}, from this total, the overall barrier is 23.5 kcal mol^{-1}.

Reactions of Xylose Protonated at O3. Earlier CPMD calculations[30] indicate that addition of a proton to O3, **41**, leads to ring opening and formation of the acyclic trihydroxy ether, **43**, shown in reaction 17. This could be a precursor to the formation of formic acid. Calculations with CBS-QB3 predict a reaction energy of $\Delta_{react}E_{0K}$(react 17) = 3.5 kcal mol^{-1} for this reaction and a cluster formation energy of $\Delta_{clust}E_{0K}$(react 17) = −5.9 kcal mol^{-1}. The transition state of this reaction has a relative energy of $\Delta_{TS}E_{0K}$(react 17) = 13.6 kcal mol^{-1}. The subsequent unimolecular decomposition to form formic acid accompanied by a 1,2-OH shift to form 4-hydroxybut-2-enal, **45**, is shown in reaction 18. The calculated energy of this reaction is $\Delta_{react}E_{0K}$(react 18) = 1.4 kcal mol^{-1}, and the transition-state energy is $\Delta_{TS}E_{0K}$(react 18) = 17.3 kcal mol^{-1}. The structures for the species in reactions 17 and 18 are shown in Figure 6. Once again, protonation leads to an apparent weakening of the C3−O3 bond as indicated by its long length, r_{C3-O3}(**41**) = 1.54 Å. The geometry of the transition state, **42**,

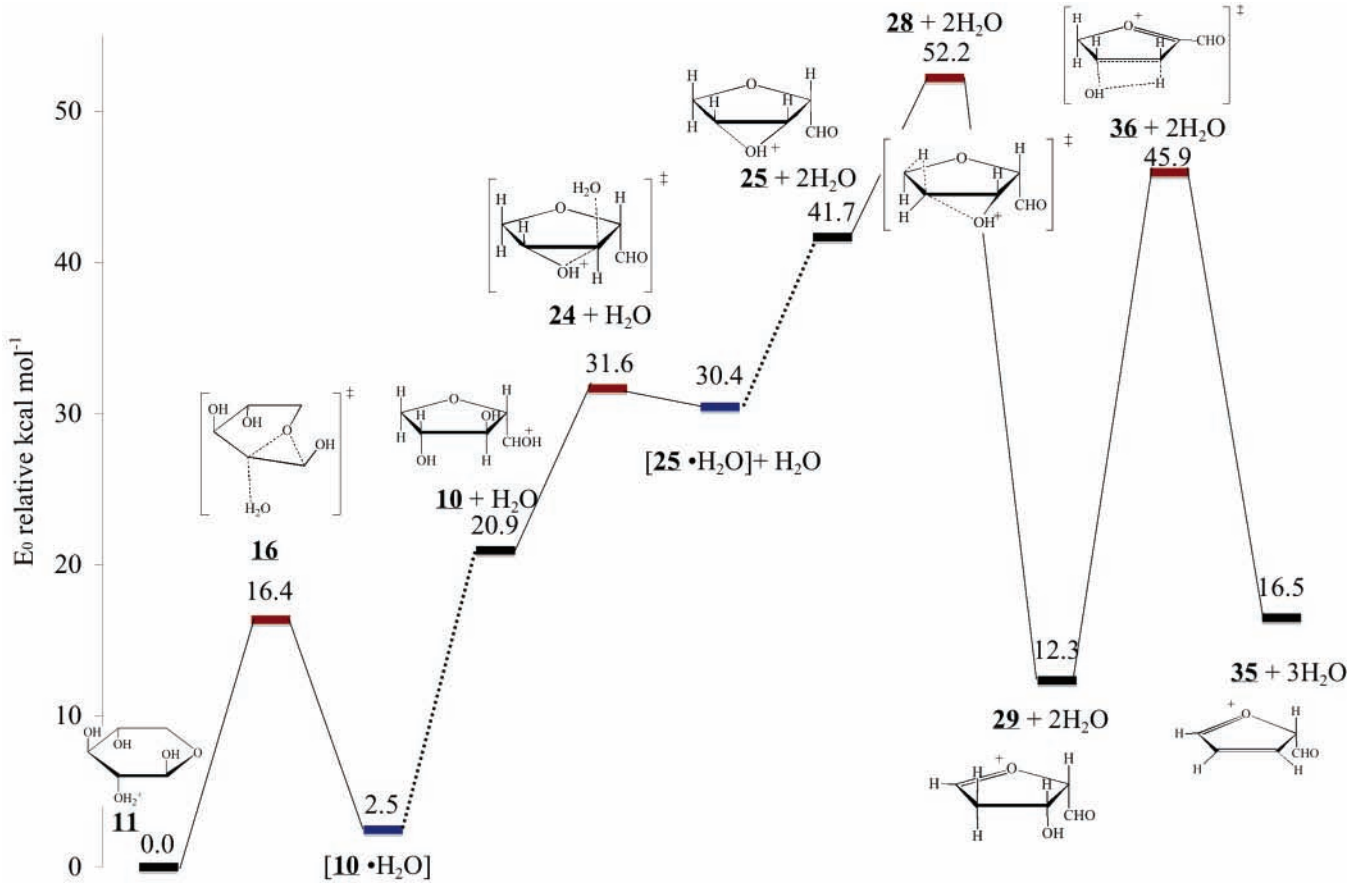

Figure 5. A plot showing the potential energies for the unimolecular conversion of xylose protonated at O2, **11**, to protontated furfural, **35**. Energies were determined with CBS-QB3. Energies of reactants are indicated with black lines, water clusters with blue lines, and transition states with red lines. The energies for reactions 3, 8, 10, and 14 are shown, though other pathways have similar energies (see text). Notice that the high barrier for reaction 14, **29** converted to **35**, can be overcome by the chemical activation energy available from crossing the barrier of reaction 10, transition state **28**. The dotted lines indicate the dissociation of water clusters formed by dehydration reactions. In solution, this energy would not be required.

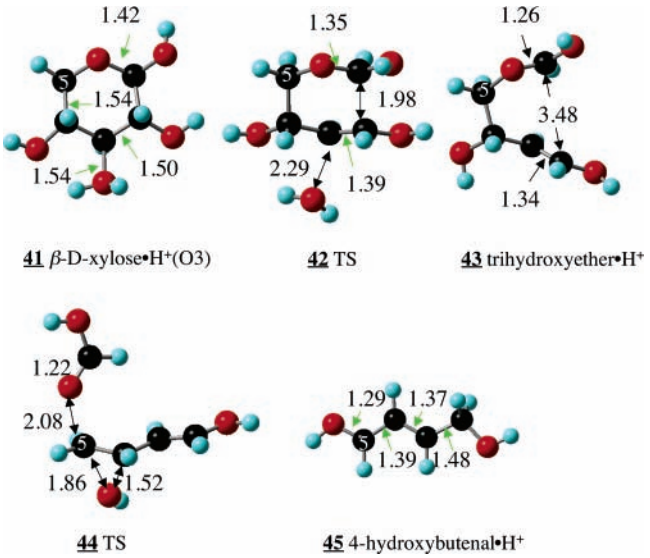

Figure 6. B3LYP/6-311G(d,p) structures for the reaction of xylose protonated at O3. Selected bond lengths are shown in Å.

IRC calculations, and the imaginary vibrational frequency show that it connects **41** and **43**. Likewise, the transition state for reaction 18 shown in Figure 6 connects **43** and **45**. The activation energies for reactions 17 and 18 are also summarized in Figure 2, showing that this mechanism is facile. These calculations present a plausible explanation for the experimental observation of formic acid from degradation of xylose in acid.

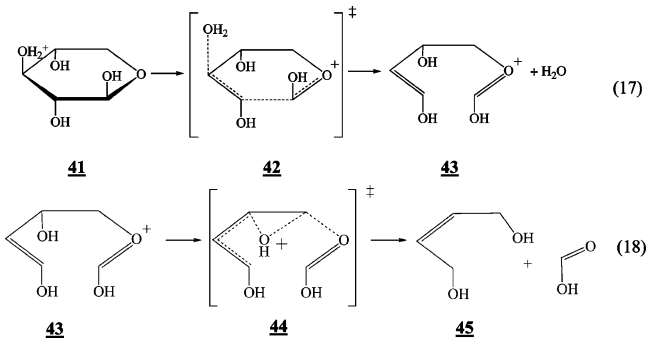

Reactions of Xylose Protonated at O4. Loss of water from xylose protonated at O4 results in ring opening to form an epoxide as shown in reaction 19. This reaction is endothermic with a reaction energy of $\Delta_{react}E_{0K}$(react 19) = 19.5 kcal mol^{-1} and a cluster formation energy of $\Delta_{clust}E_{0K}$(react 19) = 7.8 kcal mol^{-1}. As a result, even though the transition-state energy is low, $\Delta_{TS}E_{0K}$(react 19) = 11.8 kcal mol^{-1}, this reaction is unlikely because the energy of the reaction is unfavorable. In addition, no low-energy reaction for the epoxide could be found. This conclusion was also drawn from CPMD calculations.[30] The structures for reaction 19 are gathered in Figure 7, and the activation energy for this reaction is collected in Figure 2.

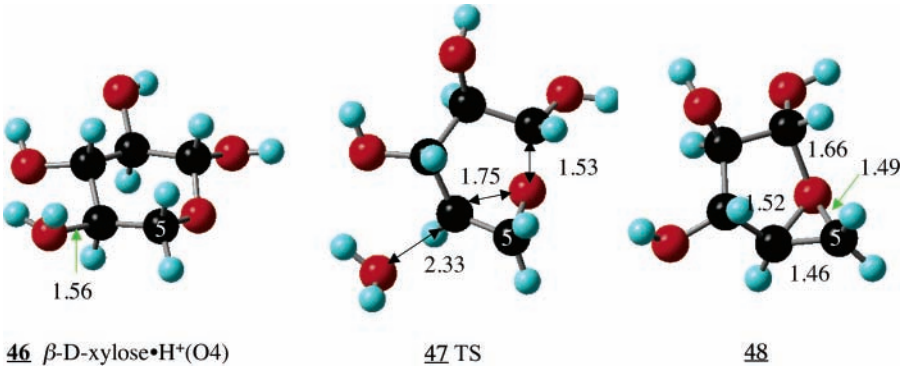

Figure 7. Calculated B3LYP/6-311G(d,p) structures for the reaction of xylose protonated at O4. Selected bond lengths are shown in Å.

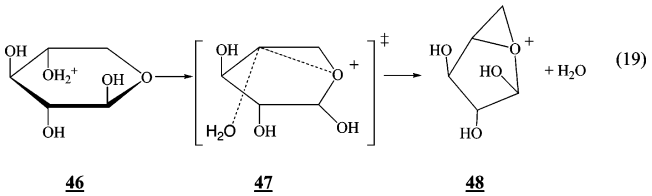

Proton Addition to O5 and Ring Opening. The first step of the mechanism for xylose destruction shown in Scheme 1 involves the opening of the pyranose ring of the sugar to form the aldose. For the unprotonated xylose, this ring opening must go through the four-centered transition, **49**, shown in reaction 20 for β-D-xylose.

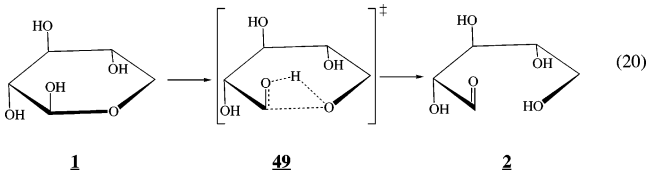

Reactions with four-centered transition states typically have high energy barriers, but experimental measurements of mutarotation seem to indicate that these barriers are low. Mutarotation, as shown in reaction 21, involves ring opening of β-D-xylose to the aldose, inversion of the carbonyl group, and ring closing to form α-D-xylose.

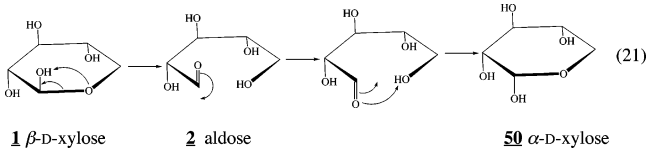

The barriers for mutarotation of sugars have been measured[54] and are roughly 15 kcal mol^{-1}, so that significant mutarotation occurs at ambient temperature.

Calculations predicted a high reaction barrier for ring opening of neutral β-D-xylose. The barrier for ring opening of the β-pyranose form of xylose is E_a = 43.5 kcal mol^{-1}. The barrier for the α-pyranose was calculated to be E_a = 46.1 kcal mol^{-1}. As discussed above, both are four-centered transition states in which the hydrogen atom on O1 is transferred to O5, while simultaneously breaking the C1−O5 bond and forming a C1−O1 double bond. The calculated structures of the transition states for ring opening of β- and α-D-xylose are shown in Figure 8, where the bond lengths for these four-centered transition states are as shown. As can be seen in Figure 8, the structures of the transition states for the two isomers are very similar. In the transition state for β-D-xylose, the C1−O5 bond length and the

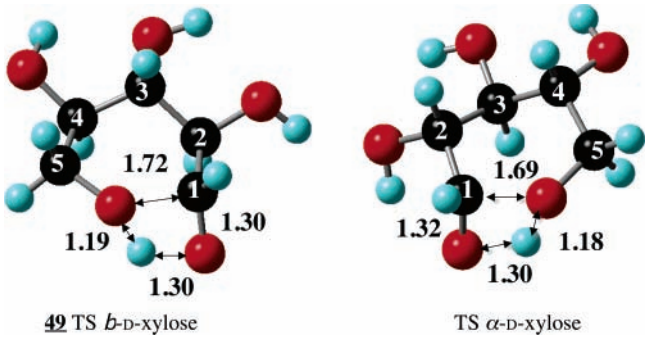

Figure 8. Structures of ring-opening transition states for neutral β-D-xylose and α-D-xylose determined using B3LYP/6-311G(d,p). Selected bond lengths are shown in Å.

O1−H1 bond length have increased to r_{C1-O5}(**49**) = 1.72 Å and r_{O1-H1}(**49**) = 1.30 Å, whereas the C1−O1 bond length has shortened to r_{C1-O1}(**49**) = 1.30 Å, and a bond has started forming between O5 and H1, r_{O5-H1}(**49**) = 1.19 Å.

Addition of a proton to the ring oxygen atom (O5) in xylose significantly lowers the energy barrier for ring opening. The barrier for β-D-xylose protonated at O5 is 9.8 kcal mol^{-1}. Because there is already a proton on O5, there is no need for a hydrogen-atom transfer in this reaction, and the transition state simply has a lengthened C1−O5 bond. Reaction 22 shows the Lewis structures of protonated xylose, **51**, the transition state, **52**, and the resulting protonated aldose, **53**. Figure 9 shows molecular geometries for these species and some of the important bond lengths in the structures. As is shown in Figure 9, adding a proton to the O5 predisposes xylose toward ring opening. The C1−O5 bond has lengthened from r_{C1-O5}(**1**) = 1.42 Å for neat xylose to r_{C1-O5}(**51**) = 1.70 Å for protonated xylose, and the C1−O1 bond has shrunk from r_{C1-O1}(**1**) = 1.40 Å to r_{C1-O1}(**51**) = 1.32 Å. This suggests that opening the protonated xylose to the aldose structure should be facile. The product from reaction 22 is formally an aldose with a proton on O1, but this proton actually forms a hydrogen bond bridge to O5 as is shown in Figure 9. The protonated aldose product, **53**, is only slightly lower in energy than the protonated xylose, **51**, with the energy of reaction 22 being $\Delta_{react}E_{0K}$(react 22) = −1.0 kcal mol^{-1}.

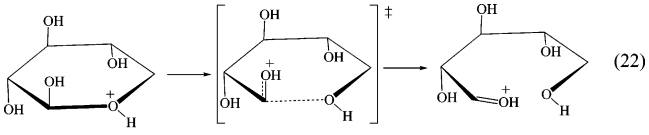

The reaction of the neutral aldose form of xylose, **2**, as proposed in Scheme 1 involves hydrogen atom transfer,

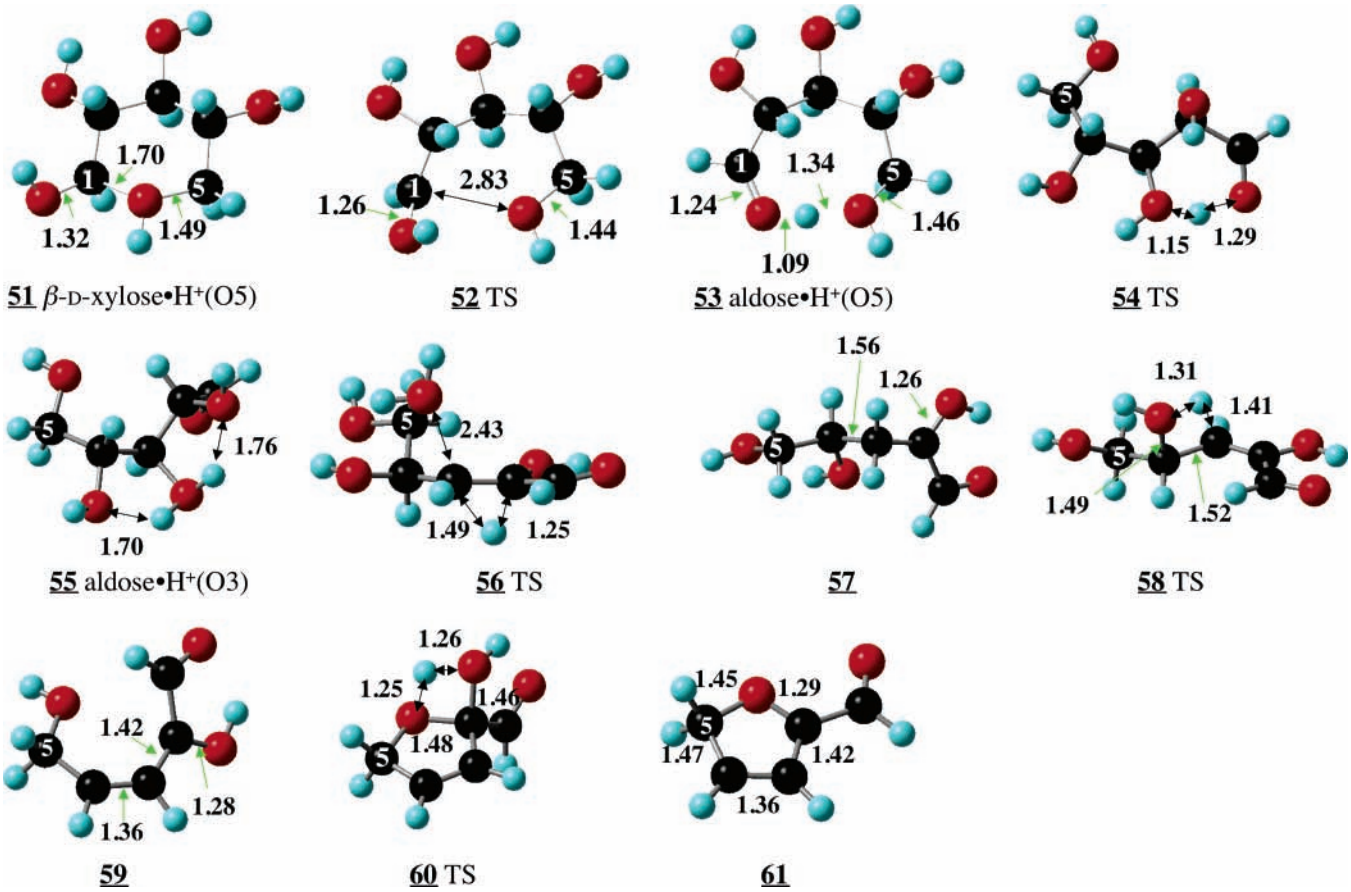

Figure 9. Structure of β-D-xylose protonated at O5 (left). Geometries were optimized at B3LYP/6-311G(d,p). Bond lengths are given in Å.

SCHEME 4

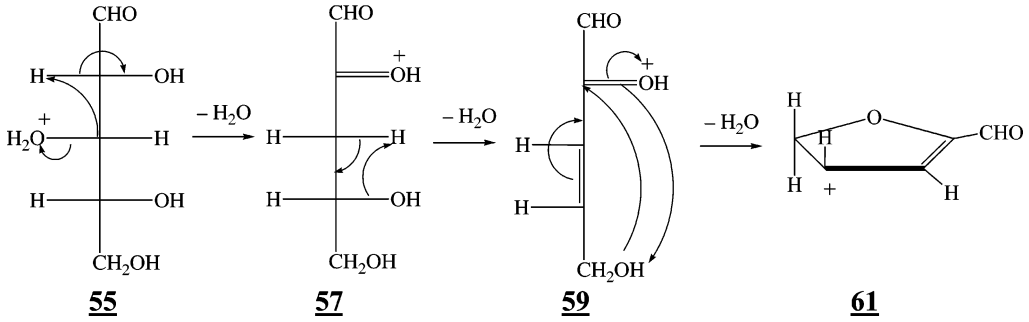

dehydration, and ring closure to give the furfural. The reactions in this scheme for neutral xylose have high reaction barriers and are unlikely. For instance, the first step in this mechanism is a tautomerization, the transfer of the C2 hydrogen to the carbonyl group in the aldose, **2**, to form the enol, **3**. The barrier for this reaction for vinyl alcohol[55] is about 55 kcal mol^{-1}, making this reaction unlikely at moderate temperatures. For instance, if one assumes a reasonable pre-exponential factor, 10^{-13} s^{-1}, the lifetimes for these reactions would be greater than 10^{27} s at 200 °C. Thus, the mechanism involving the reaction of neutral species as pictured in Scheme 1 is unlikely.

However, the calculations indicated that this mechanism would be more likely if a proton were added. The aldose protonated at O3, **55**, could react by elimination of three water molecules to give the protonated furfural, **61**, shown in Scheme 4. This mechanism is similar to the double dehydration calculated for glycerol.[53] Protonation at O3 could occur as a result of proton transfer from the bulk solution or from a direct proton transfer from O5 in the aldose formed from ring opening, ***53***, such as shown in reaction 23. The energy for this reaction is nearly thermoneutral. CBS-QB3 calculations indicate that this reaction has an energy of $\Delta_{react}E_{0K}$(react 23) = 3.2 kcal mol^{-1}, and the energy barrier is low, $\Delta_{TS}E_{0K}$(react 23) = 2.2 kcal mol^{-1}. Note that, when zero-point energy is included, the transition state, **54**, is 1.0 kcal mol^{-1} lower in energy than the product, **55**, but for potential energy only the transition state is 0.5 kcal mol^{-1} higher. The structures for **54** and **55** are collected in Figure 9.

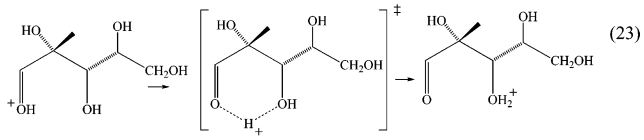

(23)

53 **54** **55**

The first step in Scheme 4 is a water loss accompanied by a hydride transfer as shown in reaction 24. The energy for the

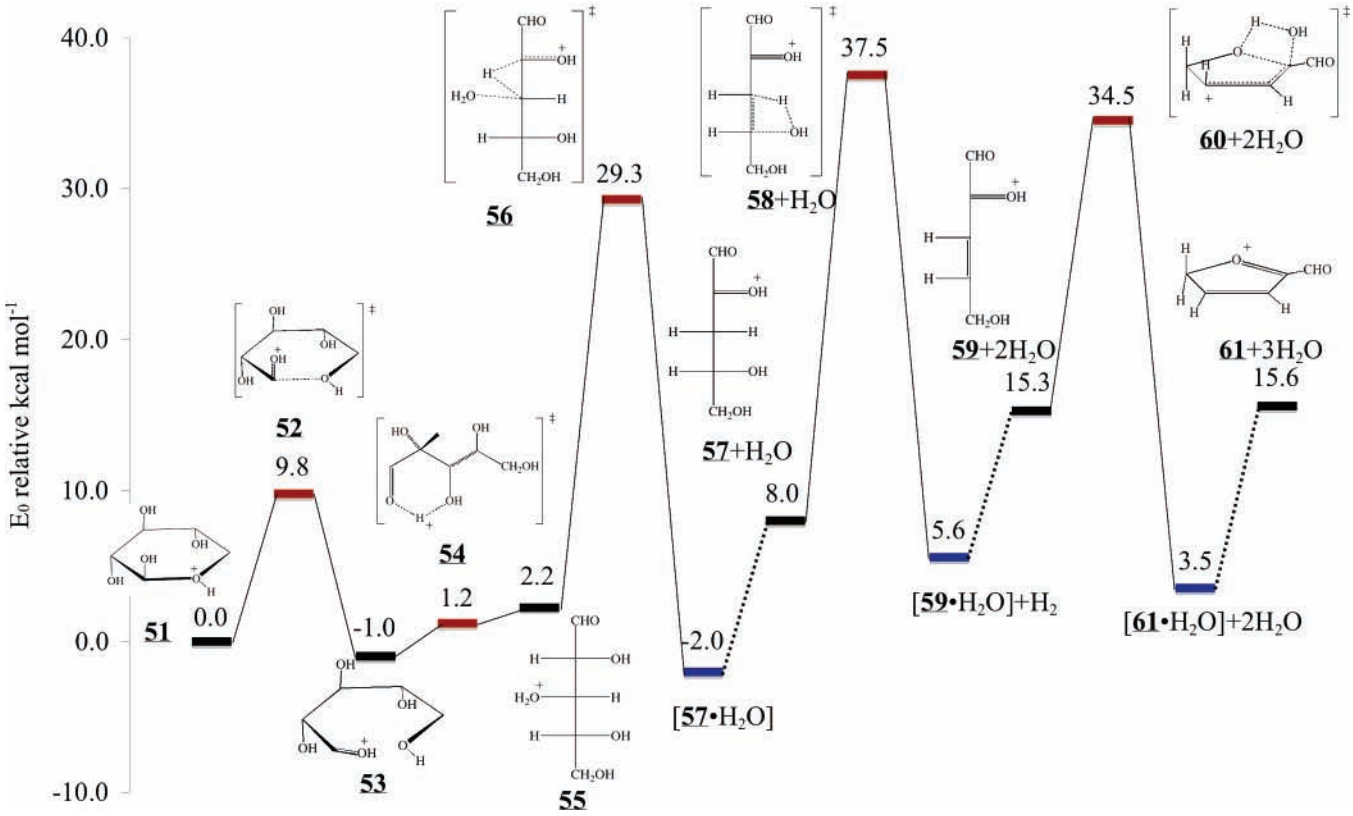

Figure 10. Potential energy plot for conversion of xylose protonated at O5 to protonated furfural. The energies were determined with CBS-QB3. Energies of reactants are shown with black lines, clusters with blue lines, and transition states with red lines. This plot contains reactions 22−26. The dotted lines indicate the dissociation of water clusters formed by dehydration reactions. In solution, this energy would not be required.

formation of **57** in reaction 24 is $\Delta_{react}E_{0K}$(react 24) = 5.8 kcal mol^{-1}, whereas the formation of the cluster is $\Delta_{clust}E_{0K}$(react 24) = − 4.2 kcal mol^{-1}. The calculated energy of the transition state relative to the reactant, **55**, is $\Delta_{TS}E_{0K}$(react 24) = 27.1 kcal mol^{-1}, and the calculated structures for **56** and **57** are collected in Figure 9. The transition state for this dehydration is anti-periplanar with the leaving H_2O and the migrating hydride on opposite sides of the molecule. As mentioned above, anti-periplanar transition states were lower in energy than the syn-periplanar transition states, where the leaving group is on the same side of the molecule as the hydride.

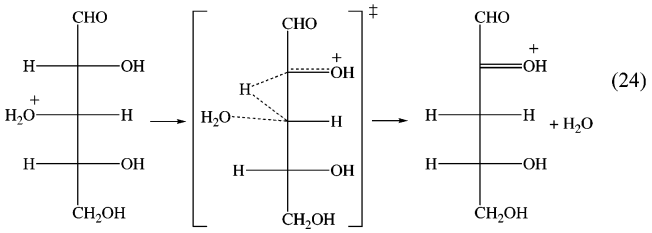

(24)

55 **56** **57**

The second dehydration occurs by a concerted loss of the OH group on C4 and a hydrogen atom on C3 as is shown in reaction 25. As mentioned above, 1,2-dehydration typically has a large energy barrier associated with a four-centered transition state.[41] However, because the double bond formed is β to the carbonyl group, the energy barrier is substantially lower. This was found to be the case for glycerol and for reactions 13−15 above. The calculated energy for reaction 25 is $\Delta_{react}E_{0K}$(react 25) = 7.3 kcal mol^{-1}, whereas the energy for the cluster formation is $\Delta_{clust}E_{0K}$(react 25) = − 2.4 kcal mol^{-1}. The calculated relative energy for the transition state is $\Delta_{TS}E_{0K}$(react 25) = 29.5 kcal mol^{-1}. Calculated structures for **58** and **59** are shown in Figure 9.

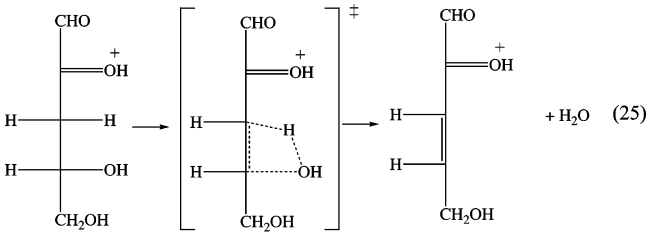

(25)

57 **58** **59**

The third step in Scheme 4 involves ring closure and dehydration as is shown in reaction 26. CBS-QB3 calculations predict that this reaction is nearly thermoneutral with an energy of $\Delta_{react}E_{0K}$(react 26) = 0.3 kcal mol^{-1}, while the formation of the product cluster has an energy of $\Delta_{clust}E_{0K}$(react 26) = 11.8 kcal mol^{-1}. The transition state has a relative energy of $\Delta_{TS}E_{0K}$-(react 26) = 19.2 kcal mol^{-1}. The calculated structures for **60** and **61** are shown in Figure 9.

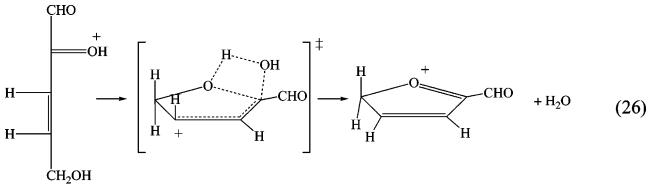

(26)

59 **60** **61**

A potential energy plot for the formation of furfural from xylose protonated at O5 is shown in Figure 10. Once again,

transitions from clustered molecules to unclustered molecules are shown with dotted lines. As can be seen, the barrier for the ring-opening step, reaction 22, is low, 9.8 kcal mol^{-1}, and the aldose is likely readily formed. However, the barriers for dehydration steps are high, 27.1, 29.5, and 19.2 kcal mol^{-1}. These barriers are especially high when compared to the barriers for furfural formation from xylose protonated at O2, Figure 5, where the barriers are less than 16.4 kcal mol^{-1}. This suggests that the mechanism for furfural formation for protonation at O2 is preferred and supports Scheme 3 over Scheme 1.

NMR Analysis. During the degradation of xylose, two pathways, resulting from the protonation of the O2 and O3 hydroxyls, are predicted to be the most productive on the basis of the models described above. The mechanisms above indicate that these two degradation pathways will produce furfural, formic acid, and a four-carbon product as shown in reaction 18. Following the pathways shown in these mechanisms, the ^{13}C label at C1 should be manifested in two new peaks. One new peak should occur at ~183 ppm, assigned to the carbonyl carbon of furfural due to the protonation of the O2 hydroxyl, whereas the second peak should occur at ~168 ppm, assigned to formic acid due to the protonation of the O3 hydroxyl.

The ^{13}C NMR spectra obtained after reacting xylose (0.067 molar) with 0.2 N H_2SO_4 at 160 °C for various times are shown in Figure 11. There is a gradual increase in the intensity of the peak at 183 ppm indicating that furfural is the major product of the xylose degradation and that the reaction pathway shown in Scheme 3 is plausible. At longer times, ^{13}C-labeled formic acid begins to appear. The appearance of ^{13}C-labeled formic may be due to the degradation of xylose after the protonation of O3 as shown in reactions 8 and 9 or possibly the decomposition of furfural.

Figure 12 shows the ^{13}C NMR spectra of xylose labeled at the C1 and C2 positions reacted with 0.2 N H_2SO_4 at 170 °C for 30 and 45 min. Again, the spectra of the xylose labeled with ^{13}C at the C1 position have the expected peaks according to Figure 3 for the carbonyls of furfural and formic acid. Labeling at the C2 position only produces a peak that is assigned to the substituted carbon of furfural and not the expected four-carbon molecule if the O3 hydroxyl was protonated as shown in reactions 17 and 18. There is no evidence of the four-carbon product, indicating that this product may be very reactive and further reacts to form the brown polymer that was observed in the reaction mixtures. The second possible explanation is that the formic acid was formed from the decomposition of furfural.

Solvation. As discussed in the Introduction, the experimental activation energy for the conversion of xylose to furfural[28,29] in a mildly acidic solution is about 30 kcal mol^{-1}. As we have shown, in the gas phase, the rate-limiting reaction step in Scheme 3 is the initial dehydration/rearrangement, reaction 3, while the rate-limiting step in Scheme 1 is one of the two dehydration steps, reactions 24 and 25. The barrier for reaction 3 is 16.4 kcal mol^{-1}, while the barriers for reactions 24 and 25 are 27.1 and 29.5 kcal mol^{-1}, respectively. Clearly, the barrier for the rate-limiting step of Scheme 3 is much lower than the experimental, solution-phase barrier. This is likely due to explicit interactions of the solvent water molecules with protonated xylose. CPMD simulations[56] of protonated xylose in the presence of explicit water molecules show that the proton on the hydroxyl groups of xylose is transferred from the xylose to the water molecules within 100 ps. This observation is consistent with bulk water having a proton affinity larger than that of xylose. As can be seen in Table 2, the calculated proton affinities for the oxygen atoms on xylose are 186−192 kcal mol^{-1}, which

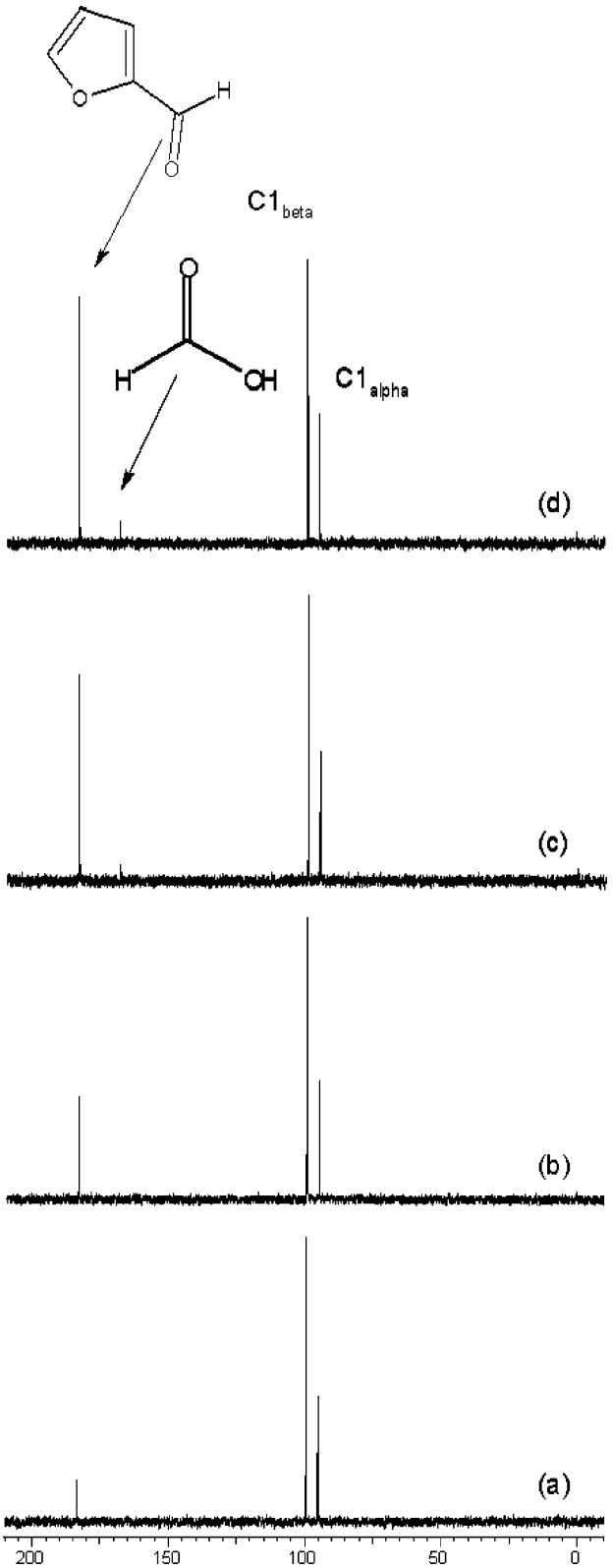

Figure 11. ^{13}C NMR spectra of C1-labeled xylose reacted with 0.2 N H_2SO_4 at 160 °C for (a) 15 min, (b) 30 min, (c) 45 min, and (d) 60 min.

is significantly larger than the experimental proton affinity[9] of a water molecule, PA(H_2O) = 165 kcal mol^{-1}. However, the proton affinity values of water clusters increase dramatically with an increase in the size of the water cluster. This is shown in Table 3, where the calculated proton affinity of water clusters increases to 220 kcal mol^{-1} for a four-water cluster. (Structures of these clusters are contained in the Supporting Information.)

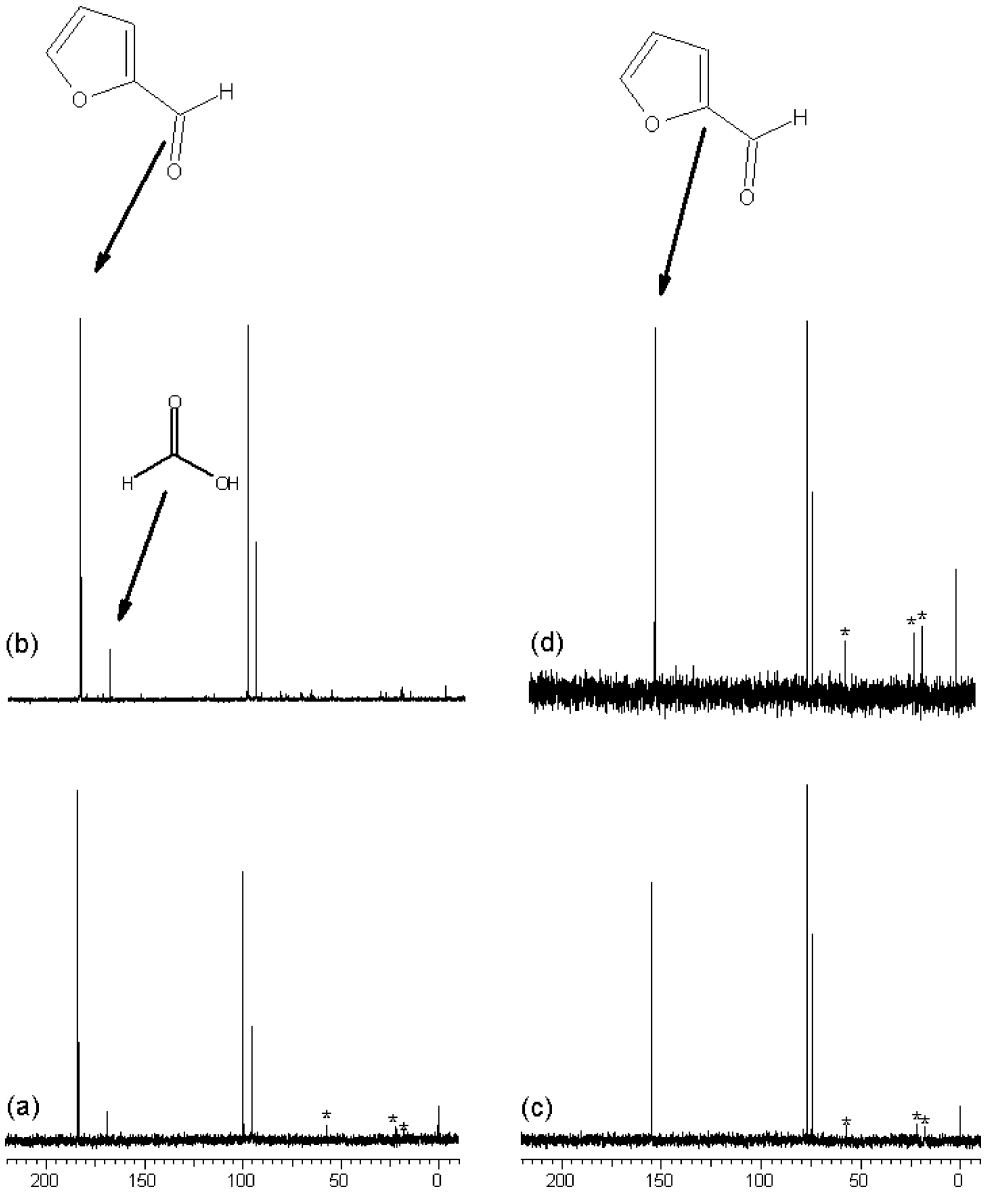

Figure 12. ^{13}C NMR spectra of xylose reacted with 0.2 N H_2SO_4 at 170 °C for (a) C1 labeled for 30 min, (b) C1 labeled for 45 min, (c) C2 labeled for 30 min, and (d) C2 labeled for 45 min. The * indicates background signals not associated with the labeled xylose materials. The sharp peak at 0 ppm is an added NMR reference material.

TABLE 3: Proton Affinities[a] of Water Clusters

species	PA
H_2O	162.5
$2H_2O$	192.2
$3H_2O$	206.6
$4H_2O$	220.2

[a] CBS-QB3.

As one moves toward bulk water, energetics would clearly favor the proton being associated with water.

To reconcile the differences in gas-phase activation energies and experimental activation energies, calculations were conducted on the reaction of protonated xylose in the presence of water molecule clusters. Because energy is required to transfer a proton from water clusters to xylose, one would expect that the addition of water clusters would increase that activation energy of xylose decomposition. To investigate this, energy barriers for the rate-limiting reactions of Scheme 3, reaction 3, and Scheme 1, reaction 24, were determined in the presence of water clusters. Initially, geometries were obtained for xylose protonated at O2 in the presence of water clusters. Because of the size of the molecules, these calculations were carried out at the B3LYP/6-311G(d,p) level. Figure 13 shows the geometries of β-D-xylose·H^+(O2) and that of this molecule clustered to one, two, and three water molecules. No attempts were made to identify the cluster structures with the lowest global energy minima. These structures were chosen for illustrative purposes. Several of the O−H bond lengths in these clusters are shown in this figure. As can be seen, when the water clusters contained two or more water molecules, the proton prefers to reside on the water cluster. Note that the bond length between O2 and the proton in the absence of a water cluster is 0.99 Å. With a single water molecule, this bond lengthens to 1.16 Å, and with two water molecules, the bond length is 1.46 Å. Furthermore, the bond length between the water and the proton decreases from 1.25 Å for a single water cluster and to 1.05 Å for a two-water cluster. For clusters containing two or more water molecules, attempts to find a stable geometry with the proton on O2 were unsuccessful. This again confirms that in solution it is more energetically favorable for the proton to be attached to water molecules.

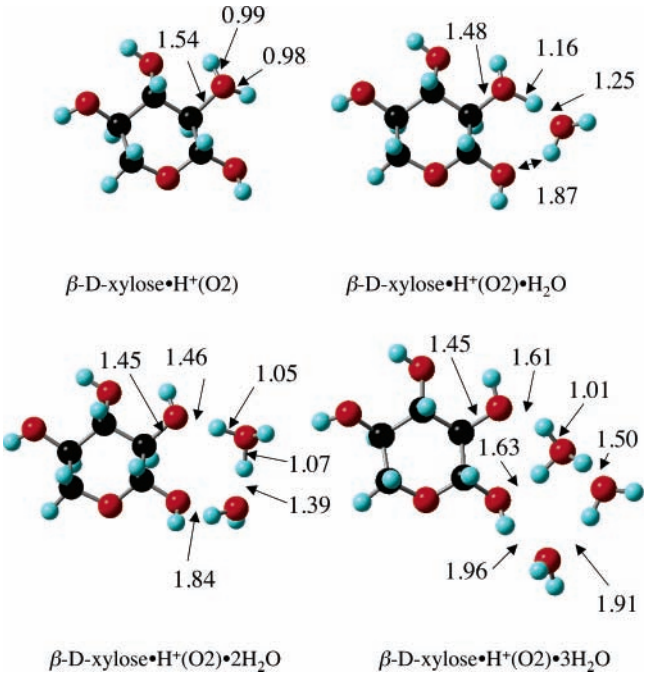

Figure 13. Structures for water clusters of xylose protonated at O2 modeled using B3LYP/6-311G(d,p).

TABLE 4: Activation[a] Energies for Reaction 3 with the Inclusion of Solvent (water)

	E_a (kcal mol^{-1})
gas phase	14.9
xyloseH$^+$•(H_2O)	32.7
xylose•(H_2O•H_3O^+)	41.3
xylose•($2H_2O$•H_3O^+)	29.9
xylose•($3H_2O$•H_3O^+)	31.3
xylose•($4H_2O$•H_3O^+)	36.4
experimental Arrhenius activation energies[b] for furfural formation	32, 30.3

[a] B3LYP/6-311G(d,p)). [b] refs 8 and 9, respectively.

With CBS-QB3, the energy barriers for reactions 3 and 24 were calculated in the presence of one water molecule in order to determine the effect of explicit water molecules on the xylose-to-furfural conversion process. Energies were calculated for single water cluster of the reactants, **11** and **55**, as well as single water clusters of the transition states, **16** and **56**. With this approach, the energy barrier for reaction 3 increases from 16.4 kcal mol^{-1} for the bare xylose to 32.4 kcal mol^{-1} for a xylose cluster with one water molecule. The barrier for reaction 24 increases from 27.1 kcal mol^{-1} for the bare molecule to 37.3 kcal mol^{-1} for the water cluster. These calculations show that including the explicit water molecule may account for the higher solution phase activation energy measured for the conversion xylose to furfural, which appears to result because of the addition energy needed for proton transfer from the solvent to xylose.

As a further test of the increase of rate-limiting reaction for Scheme 3, the barrier for reaction 3 was determined in the presence of larger water clusters. For all water clusters, the energy barrier was significantly higher than the barrier for neat protonated xylose (shown in Table 4). These energies were calculated at the B3LYP/6-311G(d,p) level, and as can be seen in Table 4, the barrier climbs from 14.9 kcal mol^{-1} for no water molecules to above 30 kcal mol^{-1} for all water clusters. Note that the lowest-energy structures were not located from the many possible conformers for these clusters, and this may account for the variability in the calculated barriers. However, the calculations appear to show that, in the limit of an infinitely large water cluster, the energy barrier will approach the experimental barrier measured in water. These calculations only provide a possible explanation for the apparent large activation energy of xylose degradation but do not speak to the interesting and complex chemistry that can occur at higher pressures in supercritical water.[57,58]

Conclusions

On the basis of calculations of the energy barriers for the dehydration of xylose, we conclude that, of the three mechanisms proposed for the formation of furfuraldehyde, Scheme 3 is the most likely. As can be seen in Figure 5, the barriers for the reaction of xylose protonated at O2, Scheme 3, are all below 17 kcal mol^{-1}. We also note that the high apparent barrier for the second to last reaction is actually lowered due to chemical activation provided by the preceding reaction. The barrier for furanose formation from protonation of xylose at O1 (Scheme 2) is 32.0 kcal mol^{-1}. This mechanism will not be competitive with the mechanism in Scheme 3. The mechanism for Scheme 1 as shown in Figure 10 for the reaction of xylose protonated at O5 has high barriers for dehydration (27.1 and 29.5 kcal mol^{-1}), and thus this mechanism is also unlikely to be competitive.

Acknowledgment. Funding for this research was provided by the Department of Energy, Office of the Biomass Program. We would also like to acknowledge the Computational Sciences Center at the National Renewable Energy Laboratory for supplying computer time.

Supporting Information Available: Ab initio and DFT calculated coordinates. This material is available free of charge via the Internet at http://pubs.acs.org.

References and Notes

(1) Sheehan, J.; Himmel, M. *Biotechnol. Prog.* **1999**, *15*, 817.
(2) Perlack, R. *Biomass as a Feedstock of a Bioenergy and Bioproducts Industry: The Technical Feasibility of a Billion Ton Annual Supply*; ORNL and USDA; U.S. Government Printing Office: Washington, DC, 2005.
(3) Grohmann, K.; Himmel, M. E. Enzymes for Fuels and Chemical Feedstocks. In *Enzymes in Biomass Conversion*; Leatham, C. F., Himmel, M. E., Eds.; American Chemical Society: Washington, DC, 1991.
(4) Sjostrom, E. *Wood Chemistry: Fundamentals and Applications*; Academic Press: San Diego, 1993.
(5) Mason, P. E.; Neilson, G. W.; Enderby, J. E.; Saboungi, M. L.; Brady, J. W. *J. Phys. Chem. B* **2005**, *109*, 13104.
(6) Momany, F. A.; Appell, M.; Willett, J. L.; Bosma, W. B. *Carbohydr. Res.* **2005**, *340*, 1638.
(7) Appell, M.; Willett, J. L.; Momany, F. A. *Carbohydr. Res.* **2005**, *340*, 459.
(8) Corchado, J. C.; Sanchez, M. L.; Aguilar, M. A. *J. Am. Chem. Soc.* **2004**, *126*, 7311.
(9) Appell, M. D.; Momany, F. A.; Willett, J. L. *Abstr. Pap. Am. Chem. Soc.* **2003**, *225*, U256.
(10) Talon, U.; Smith, L. J.; Brady, J. W.; Lewis, B. A.; Copley, J. R. D.; Price, D. L.; Saboungi, M. L. *J. Phys. Chem. B* **2004**, *108*, 5120.
(11) Smith, L. J.; Price, D. L.; Chowdhuri, Z.; Brady, J. W.; Saboungi, M. L. *J. Chem. Phys.* **2004**, *120*, 3527.
(12) Momany, F. A.; Appell, M.; Strati, G.; Willett, J. L. *Carbohydr. Res.* **2004**, *339*, 553.
(13) Molteni, C.; Parrinello, M. *J. Am. Chem. Soc.* **1998**, *120*, 2168.
(14) Molteni, C.; Parrinello, M. *Chem. Phys. Lett.* **1997**, *275*, 409.
(15) Cramer, C. J.; Truhlar, D. G.; French, A. D. *Carbohydr. Res.* **1997**, *298*, 1.
(16) Barrows, S. E.; Cramer, C. J.; Dulles, F. J.; French, A. D.; Truhlar, D. G. *Abstr. Pap. Am. Chem. Soc.* **1995**, *209*, 111.
(17) Cramer, C. J.; Truhlar, D. G. *J. Am. Chem. Soc.* **1993**, *115*, 5745.
(18) Grohmann, K.; Torget, R.; Himmel, M. *Biotechnol. Bioenerg. Symp.* **1985**, *15*, 59.
(19) Grethlein, H. E. *Biotechnol. Bioeng.* **1978**, *20*, 503.
(20) Saeman, J. *Ind. Eng. Chem.* **1945**, *37*, 43.

(21) Dunlop, A. P. *Ind. Eng. Chem.* **1948**, *40*, 204.
(22) Hurd, C. D.; Isenhour, L. L. *J. Am. Chem. Soc.* **1932**, *54*, 317.
(23) Harris, D. W.; Feather, M. S. *Carbohydr. Res.* **1973**, *30*, 359.
(24) Feather, M. S.; Harris, D. W.; Nichols, S. B. *J. Org. Chem.* **1972**, *37*, 1606.
(25) Feather, M. S. *Tetrahedron Lett.* **1970**, *48*, 4143.
(26) Antal, M. J.; Leesomboon, T.; Mok, W. S.; Richards, G. N. *Carbohydr. Res.* **1991**, *217*, 71.
(27) Shafizadeh, F.; McGinnis, G. D.; Philpot, C. W. *Carbohydr. Res.* **1972**, *25*, 23.
(28) Root, D. F.; Saeman, J. F.; Harris, J. F. *Forest Prod. J.* **1959**, 158.
(29) Garrett, E. R.; Dvorchik, B. H. *J. Pharm. Sci.* **1969**, *58*, 813.
(30) Qian, X.; Nimlos, M. R.; Johnson, D. K.; Himmel, M. E. *App. Biochem. Biotechnol.* **2005**, *121*−*124*, 989.
(31) Marx, D.; Parrinello, M. *Z. Phys. B: Condens. Matter* **1994**, *95*, 143.
(32) Frisch, M. J.; Trucks, G. W.; Schlegel, H. B.; Scuseria, G. E.; Robb, M. A.; Cheeseman, J. R.; Montgomery, J. A., J.; Vreven, T.; Burant, J. C.; Millam, J. M.; Iyengar, S. S.; Tomasi, J.; Barone, V.; Mennucci, B.; Cossi, M.; Scalmani, G.; Rega, N.; Petersson, G. A.; Nakatsuji, H.; Hada, M.; Ehara, M.; Toyota, K.; Fukuda, R.; Hasegawa, J.; Ishida, M.; Nakajima, T.; Honda, Y.; O. Kitao; Nakai, H.; Klene, M.; Li, X.; Knox, J. E.; Hratchian, H. P.; J. B. Cross; Adamo, C.; Jaramillo, J.; Gomperts, R.; Stratmann, R. E.; Yazyev, O.; Austin, A. J.; Cammi, R.; Pomelli, C.; Ochterski, J. W.; Ayala, P. Y.; Morokuma, K.; Voth, G. A.; Salvador, P.; Dannenberg, J. J.; Zakrzewski, V. G.; Dapprich, S.; Daniels, A. D.; Strain, M. C.; Farkas, O.; Malick, D. K.; Rabuck, A. D.; Raghavachari, K.; Foresman, J. B.; Ortiz, J. V.; Cui, Q.; Baboul, A. G.; Clifford, S.; Cioslowski, J.; Stefanov, B. B.; Liu, G.; Liashenko, A.; Piskorz, P.; Komaromi, I.; Martin, R. L.; Fox, D. J.; Keith, T.; Al-Laham, M. A.; Peng, C. Y.; Nanayakkara, A.; Challacombe, M.; Gill, P. M. W.; Johnson, B.; Chen, W.; Wong, M. W.; Gonzalez, C.; Pople, J. A. *Gaussian 03*; Gaussian, Inc.: Wallingford, CT, 2001.
(33) Montgomery, J. A.; Frisch, M. J.; Ochterski, J. W.; Petersson, G. A. *J. Chem. Phys.* **1999**, *110*, 2822.
(34) Curtiss, L. A.; Raghavachari, K.; Trucks, G. W.; Pople, J. A. *J. Chem. Phys.* **1991**, *94*, 7221.
(35) Foresman, J. B.; Frisch, A. *Exploring Chemistry with Electronic Structure Methods*; Gaussian, Inc.: Pittsburgh, PA, 1995.
(36) Hodgson, D.; Zhang, H. Y.; Nimlos, M. R.; McKinnon, J. T. *J. Phys. Chem. A* **2001**, *105*, 4316.
(37) Basch, H.; Hoz, S. *J. Phys. Chem. A* **1997**, *101*, 4416.
(38) Bach, R. D.; Glukhovtsev, M. N.; Gonzalez, C.; Marquez, M.; Estevez, C. M.; Baboul, A. G.; Schlegel, H. B. *J. Phys. Chem. A* **1997**, *101*, 6092.
(39) Dobbs, K. D.; Dixon, D. A. *J. Phys. Chem.* **1994**, *98*, 12584.
(40) Oie, T.; Topol, I. A.; Burt, S. K. *J. Phys. Chem.* **1995**, *99*, 905.
(41) Nimlos, M. R.; Blanksby, S. J.; Ellison, G. B.; Evans, R. J. *J. Anal. Appl. Pyrolysis* **2003**, *66*, 3.
(42) Gonzalez, C.; Schlegel, H. B. *J. Phys. Chem.* **1990**, *94*, 5523.
(43) Gonzalez, C.; Schlegel, H. B. *J. Chem. Phys.* **1989**, *90*, 2154.
(44) Barrows, S. E.; Dulles, F. J.; Cramer, C. J.; French, A. D.; Truhlar, D. G. *Carbohydr. Res.* **1995**, *276*, 219.
(45) Hordvik, A. *Acta Chem. Scand.* **1971**, *25*, 2175.
(46) Zaman, N.; Darlow, S. F. *J. Bangladesh Acad. Sci.* **1980**, *10*, 177.
(47) Ma, B. Y.; Schaefer, H. F.; Allinger, N. L. *J. Am. Chem. Soc.* **1998**, *120*, 3411.
(48) Appell, M.; Strati, G. L.; Willett, J. L.; Momany, F. A. *Carbohydr. Res.* **2004**, *339*, 537.
(49) Collins, P. M.; Ferrier, R. J. *Monosaccharides, Thir Chemistry and Their Roles in Natural Products*; John Wiley and Sons Ltd.: West Sussex, England, 1995.
(50) Hunter, E. P. L.; Lias, S. G. *J. Phys. Chem. Ref. Data* **1998**, *27*, 413.
(51) Lewis, D.; Keil, M.; Sarr, M. *J. Am. Chem. Soc.* **1974**, *96*, 4398.
(52) Tsang, W. *Int. J. Chem. Kinet.* **1976**, *8*, 173.
(53) Nimlos, M. R.; Blanksby, S. J.; Qian, X. H.; Himmel, M. E.; Johnson, D. K. *J. Phys. Chem. A* **2006**, *110*, 6145.
(54) Pigman, W.; Isbell, H. S. Mutarotation of Sugars in Solution: Part I History, Basic Kinetics, and Composition of Sugar Solutions. In *Advances in Carbohydrate Chemistry and Biochemistry*; Elsevier: London, 1968; Vol. 23, p 11.
(55) Teixeira-Dias, J. J. C.; Furlani, T. R.; Shores, K. S.; Garvey, J. F. *Phys. Chem. Chem. Phys.* **2003**, *5*, 5063.
(56) Qian, X. H.; Nimlos, M. R.; Davis, M.; Johnson, D. K.; Himmel, M. E. *Carbohydr. Res.* **2005**, *340*, 2319.
(57) Penninger, J. M. L.; Kersten, R. J. A.; Baur, H. C. L. *J. Supercrit. Fluids* **1999**, *16*, 119.
(58) Narayan, R.; Antal, M. J. *J. Am. Chem. Soc.* **1990**, *112*, 1927.